iScience

CellPress
OPEN ACCESS

Article

Specificity and efficiency of tamoxifen-mediated Cre induction is equivalent regardless of age

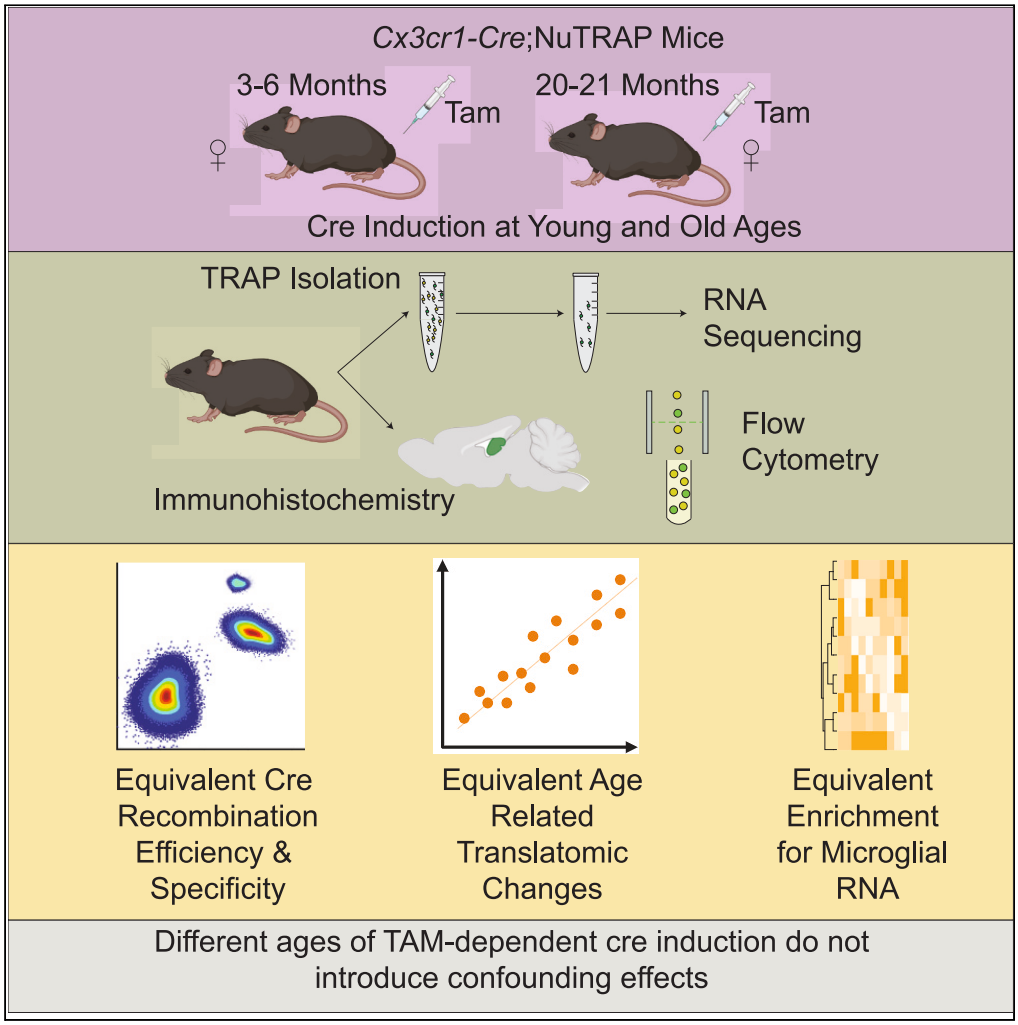

Collyn M. Kellogg, Kevin Pham, Sunghwan Ko, ..., Ana J. Chucair-Elliott, Sarah R. Ocañas, Willard M. Freeman

bill-freeman@omrf.org

Highlights

Specificity of *Cx3cr1*^{ERT2} is equivalent in young and old mice

High efficiency of Cre induction is observed across ages

NuTRAP ribosome and nuclei tagging can be performed across ages

Systemic approach for evaluating Cre induction at different ages

Kellogg et al., iScience 26, 108413
December 15, 2023
https://doi.org/10.1016/j.isci.2023.108413

iScience

CellPress
OPEN ACCESS

Article

Specificity and efficiency of tamoxifen-mediated Cre induction is equivalent regardless of age

Collyn M. Kellogg,[1,2] Kevin Pham,[1] Sunghwan Ko,[1,6] Jillian E.J. Cox,[1,6] Adeline H. Machalinski,[1] Michael B. Stout,[3] Amanda L. Sharpe,[4,6] Michael J. Beckstead,[3,5] Ana J. Chucair-Elliott,[1] Sarah R. Ocañas,[1,6,7] and Willard M. Freeman[1,2,5,6,8,*]

SUMMARY

Temporally controlling Cre recombination through tamoxifen (Tam) induction has many advantages for biomedical research. Most studies report early post-natal/juvenile (<2 m.o.) Tam induction, but age-related neurodegeneration and aging studies can require Cre induction in older mice (>12 m.o.). While anecdotally reported as problematic, there are no published comparisons of Tam-mediated Cre induction at early and late ages. Here, microglial-specific *Cx3cr1*^{creERT2} mice were crossed to a floxed NuTRAP reporter to compare Cre induction at early (3–6 m.o.) and late (20 m.o.) ages. Specificity and efficiency of microglial labeling at 21–22 m.o. were identical in mice induced with Tam at early and late ages. Age-related microglial translatomic changes were also similar regardless of Tam induction age. Each Cre and flox mouse line should be independently validated, however, these findings demonstrate that Tam-mediated Cre induction can be performed even into older mouse ages and should be generalizable to other inducible Cre models.

INTRODUCTION

The development of the Cre-*loxP* system,[1,2] with subsequent integration[3] and refinement[4] of a Cre bound to a mutated estrogen receptor (*ERT2*) allows for temporally controlled induction of cre recombination with tamoxifen (Tam) administration.[4–6] When Cre-ERT2 expressing mice are crossed to mice with *loxP* sites flanking a stop codon or desired gene, induction of the cre recombinase via Tam injection activates or suppresses the transgene, respectively.[7,8] Including a gene promoter of a cell type-specific gene upstream of the Cre-ERT2 gene can combine cell specificity and temporal control.[9,10] This system has been widely adopted and utilized across biomedical research. While a plethora of reports describe the validation of different Cre-ERT2 expressing mouse lines and examine the effects of altered transgene expression, most studies report induction of Cre recombination at young/adolescent age (<2–3 m.o.).

In aging research and age-related neurodegeneration studies, experimental designs that induce Cre recombinase at old ages can be advantageous. A long-standing hypothesis in aging research is that expression of certain genes is positively adaptive at young age until late age, where it becomes maladaptive.[11] In neurodegeneration studies, neuroinflammatory responses may be prodromally beneficial to contain disease spread but deleterious over longer periods, contributing to disease progression.[12–17] Thus, experimental designs where Tam induction of Cre recombinase is performed in older mice are warranted. However, to our knowledge, there are no reports comparing *in vivo* cre induction in young and old mice.

Tam is metabolized by cytochrome P450 into the metabolites N-desmethyltamoxifen, 4-hydroxytamoxifen, endoxifen, and norendoxifen, with 4-hydroxytamoxifen being the most potent metabolite.[18,19] Variability in Tam metabolism and clearance have been reported based on age, dosage, treatment duration, genetic differences, sex, and other factors, leading to different half-lives and potencies of the metabolites.[19–21] As well, epigenetics or other unanticipated cellular changes could potentially alter recombination efficiency. Due to these differences, there could be a concern that mice of different ages could demonstrate differences in Tam dependent cre induction that could confound studies.

As a test platform to asses Tam-mediated induction of microglia in the brain we examined a number of Cre-ERT2 linse,[22] such as *Hexb-cre*,[23] *P2ry12-cre*,[24] *Tmem119-cre*,[25] *Sall1-cre*, and *Cx3cr1-cre*.[26,27] *Cx3cr1-cre* drivers have been the most widely used with efficient recombination

[1]Genes & Human Disease Program, Oklahoma Medical Research Foundation, Oklahoma City, OK, USA
[2]Department of Biochemistry & Molecular Biology, University of Oklahoma Health Sciences Center, Oklahoma City, OK, USA
[3]Aging & Metabolism Program, Oklahoma Medical Research Foundation, Oklahoma City, OK, USA
[4]Department of Pharmaceutical Sciences, University of Oklahoma Health Sciences Center, Oklahoma City, OK, USA
[5]Oklahoma City Veterans Affairs Medical Center, Oklahoma City, OK, USA
[6]Neuroscience Graduate Program, University of Oklahoma Health Sciences Center, Oklahoma City, OK, USA
[7]Department of Physiology, University of Oklahoma Health Sciences Center, Oklahoma City, OK, USA
[8]Lead contact
*Correspondence: bill-freeman@omrf.org
https://doi.org/10.1016/j.isci.2023.108413

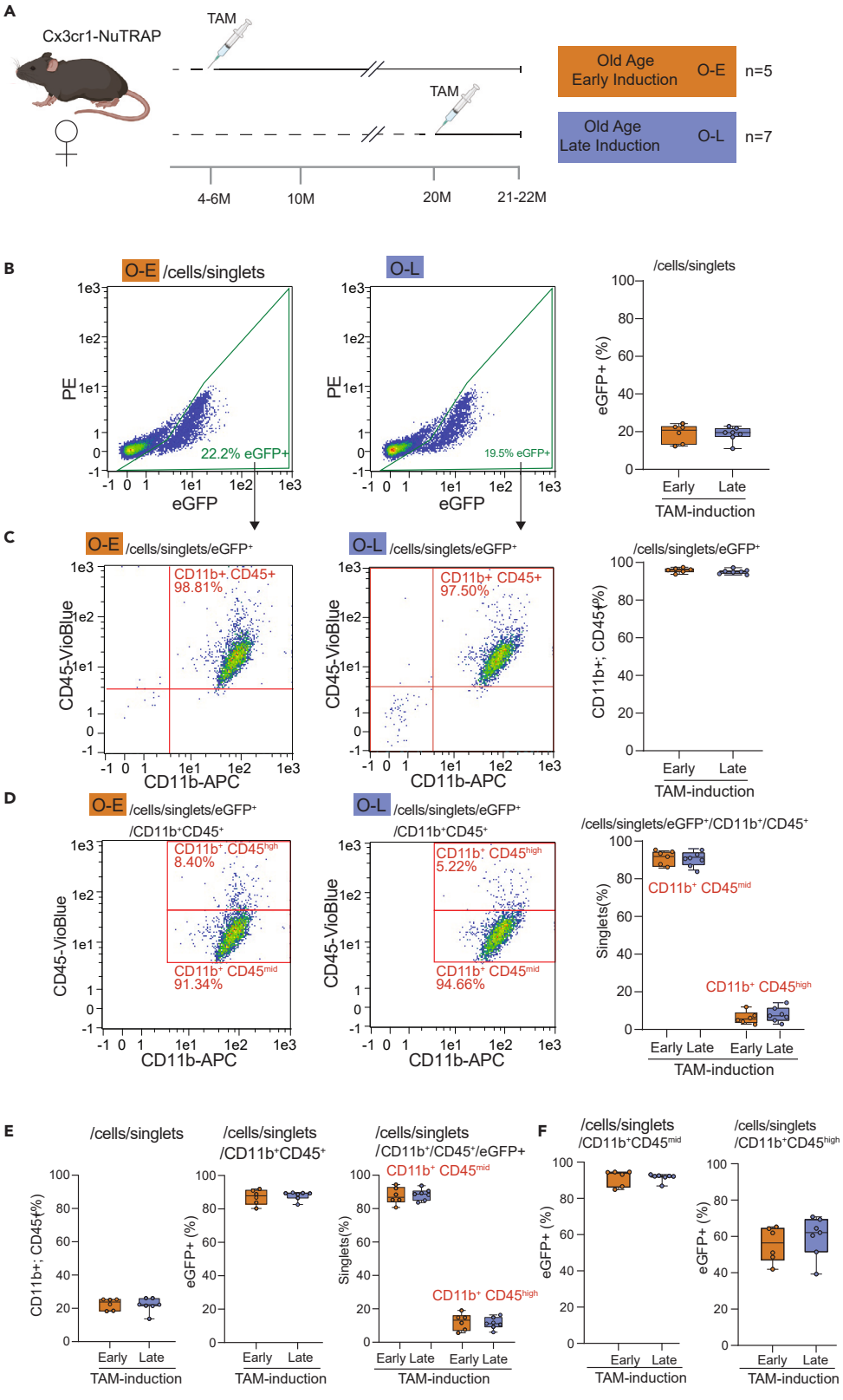
A
Cx3cr1-NuTRAP
TAM
TAM
4-6M
10M
20M
21-22M
Old Age Early Induction
O-E
n=5
Old Age Late Induction
O-L
n=7
B
O-E /cells/singlets
O-L
PE
eGFP
22.2% eGFP+
19.5% eGFP+
/cells/singlets
eGFP+ (%)
Early
Late
TAM-induction
C
O-E /cells/singlets/eGFP+
O-L /cells/singlets/eGFP+
CD45-VioBlue
CD11b-APC
CD11b+ CD45+
98.81%
97.50%
/cells/singlets/eGFP+
CD11b+; CD45+(%)
D
O-E /cells/singlets/eGFP+
/CD11b+CD45+
O-L /cells/singlets/eGFP+
/CD11b+CD45+
CD11b+ CD45high
8.40%
5.22%
CD11b+ CD45mid
91.34%
94.66%
/cells/singlets/eGFP+/CD11b+/CD45+
Singlets(%)
CD11b+ CD45mid
CD11b+ CD45high
Early Late
Early Late
TAM-induction
E
/cells/singlets
/cells/singlets
/CD11b+CD45+
/cells/singlets
/CD11b+/CD45+/eGFP+
CD11b+; CD45+(%)
eGFP+ (%)
Singlets(%)
CD11b+ CD45mid
CD11b+ CD45high
Early Late
TAM-induction
F
/cells/singlets
/CD11b+CD45mid
/cells/singlets
/CD11b+CD45high
eGFP+ (%)
Early Late
TAM-induction

Figure 1. Cell labeling and efficiency are equivalent regardless of TAM induction age

(A) Experimental design of early Tam induction (4–6 m.o.) and late Tam induction (20 m.o.) in Cx3cr1-NuTRAP mice followed by brain collection for both groups at 21–22 m.o.

(B) Single cell suspensions generated by enzymatic and mechanical dissociation of half brain cortex were gated on eGFP+ singlets, with ~20% observed in both young and old induction mice.

(C) Of these eGFP+ singlets nearly all (~98%) were double-positive for CD11b and CD45.

(D) Further dividing this triple positive population ($CD11b^+/CD45^+/EGFP^+$) into prototypical microglia ($CD45^{mid}/CD11b^+$) and other resident macrophages ($CD45^{high}/CD11b^+$) revealed equivalent populations.

(E) Using the same data, the inverse analysis was performed to determine percentage of all cells $CD11b^+/CD45^+$, of which nearly all were $eGFP^+$, the vast majority of which were $CD11b^+/CD45^+/EGFP^+$.

(F) ~90% percent of $CD11b+CD45^{mid}$ singlets were eGFP+, indicative of high efficiency of Cre recombination for microglia in our model with both ages of Tam induction. Similar efficiency of recombination was observed at both ages of induction when analyzing %eGFP in $CD45^{high}/CD11b^+$ cells (putative macrophages). Data are presented as mean ± S.E.M.

and almost exclusive targeting of microglia reported.[27,28] Use of a YFP-bound *Cx3cr1-cre* showed up to 98% of YFP positive cells were Iba1 positive microglia with no neuronal cell labeling.[27,28] With this mouse line, there is some labeling of circulating monocytes and border associated macrophages; however, with the long lifespan of microglial cells, and high turnover of peripheral monocytes, labeled circulating macrophages are cleared 2–4 weeks after Cre induction and the bone marrow progenitors do not demonstrate recombination.[22,27–30] For the present studies, to compare different ages of Tam induction, $Cx3cr1^{creERT222}$ mice were crossed to mice with a floxed NuTRAP allele (nuclear tagging and translating ribosome affinity purification)[31] which tags nuclei with biotin/mCherry and ribosomes with eGFP[32,33] similar to Ribotag protocols.[34] These tags can be used for INTACT (Isolation of Nuclei TAgged in specific Cell Types)[35] isolation of nuclei or TRAP (translating ribosome affinity purification)[36] isolation of ribosomes to obtain cell type-specific nucleic acids (DNA and RNA, respectively) from cellularly heterogeneous tissues. The fluorescent tags can be also used for imaging, cell sorting, and flow cytometry.[32,37]

This study investigates whether the effects of treating these mice with Tam at different ages (3–6 and 20 m.o.) have an impact on Cre efficiency and specificity, and ability to detect age-related translatome changes in *Cx3cr1-cre*;NuTRAP mice.[32] We have used this experimental design of TRAP and INTACT and a floxed NuTRAP mouse model to better understand the transcriptional and epigenetic changes with age in various cell types.[38–40] The key findings from this study are that age of Tam induction had no significant effect on the efficiency or specificity of Cre recombinase induction, isolation of microglial specific translatome profiles, or the ability to identify age-related microglial translatomic alterations. These results demonstrate that experimental designs utilizing early life and late-life Tam administration are valid approaches for microglial studies and most likely generalizable to other inducible Cre mouse models.

RESULTS

Microglial cell labeling specificity and efficiency are equivalent despite the age of cre induction

Single cell suspensions from aged (21–22 m.o.) cortex were collected from mice induced with Tam at either early (3–6 m.o., n = 6, 4 females, 2 males) or late (20 m.o., n = 7, 5 females, 2 males) age (Figure 1A) and stained for microglial markers CD11b and CD45. Regardless of induction age, ~20% of all cell singlets were $eGFP^+$ from the NuTRAP transgene (Figure 1B). Over 95% of $eGFP^+$ cells were CD11b/CD45 double-positive, (Figure 1C) indicating that the Cre recombination was equally specific for microglia at both ages of induction. One caveat of using CD45 as a microglial marker is that other resident myeloid cell types, such as macrophages, have surface expression of CD11b and CD45; however, there is the distinction between microglia and macrophages based on surface expression level of CD45.[41–43] Cells were further gated by $CD11b^+$ $CD45^{mid}$ and $CD11b^+$ $CD45^{high}$, with both induction ages having similar percentages (<10%) of $CD45^{high}$ $eGFP^+$ cells, demonstrating an equally microglial specific recombination (Figure 1D). No differences in the $CD45^{mid}$ $eGFP^+$ cell population by age of induction were observed. To compare efficiency of Cre induction, the inverse gating strategy was used where the $CD11b^+$ $CD45^+$ singlets were assessed for eGFP positivity (Figure 1E) with the vast majority of $CD11b^+$ $CD45^{mid}$ cells being $eGFP^+$, in agreement with other reports of efficiency.[44] At greater detail, using the efficiency of eGFP labeling as a surrogate for Cre recombination efficiency, of the $CD11b^+$ $CD45^{mid}$ cells ~90% were $eGFP^+$, while in $CD11b^+$ $CD45^{high}$ cells, ~60% were $eGFP^+$ indicating that recombination efficiency is less in these macrophages (Figure 1F). Extending these analyses, IHC analysis of brain tissue sections in the hippocampus showed co-localization of both NuTRAP reporter proteins, eGFP and mCherry in $CD11b^+$ cells (Figure 2), consistent with microglial identity. The pattern of recombination was undistinguishable between samples of mice subjected to early or late Tam induction. Together, these data suggest that Tam induction of *Cx3cr1*-NuTRAP mice during early or late age results in similar cell specificity and efficiency of Cre recombination in microglia.

Age of cre induction does not alter TRAP isolation of microglial-specific RNA efficiency

Once establishing specificity and efficiency of recombination of the NuTRAP allele at both ages of Tam induction, we set out to determine if the downstream TRAP isolation of RNA demonstrated similar profiles. The NuTRAP allele labels ribosomes with eGFP, which can then be isolated to collect cell type-specific RNA for further analysis[32] (Figure 3A). A schematic of the NuTRAP isolation method can be found in Figure S1. To determine the consistency of microglial specific RNA enrichment at different time points of Tam administration, mice were treated at an early age (3 m.o) and collected at young age (4 m.o., n = 5, 5 female, Young Age—Early Induction) or were Tam treated early (at 3–6 m.o,

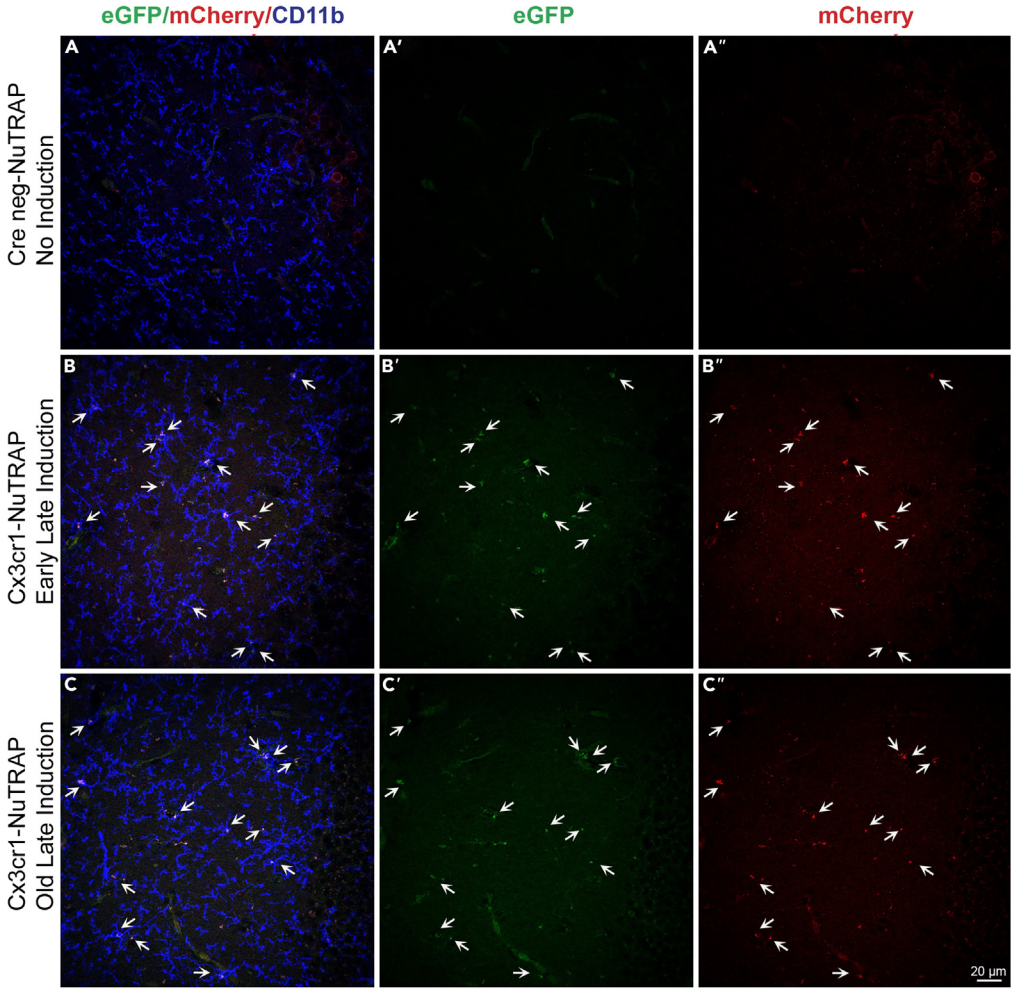

Figure 2. DNA Recombination in the brain of old Cx3cr1-NuTRAP mice subjected to tamoxifen treatment during early and late life

Cx3cr1-cre^{+} NuTRAP^{+}(Cx3cr1-NuTRAP) mice were treated with Tam at 4–6 m.o. (early induction) or 20 m.o. (late induction). At 21–22 m.o., brains were harvested and processed for immunohistochemical analysis of microglial recombination. Frozen tissue sections were immunostained with antibodies against mCherry and CD11b. Representative confocal fluorescent microscopy images of sagittal brain sections show that unlike Cre negative counterparts (controls) (a–a′′), Cx3cr1-NuTRAP brains displayed colocalization of eGFP (green signal), mCherry (red signal), and CD11b (blue signal) following early (b–b′′) and late (c–c′′) Tam administration regimes. The area imaged for each sample encompasses the dentate gyrus of the hippocampus. The scale bar depicts 20 μm.

n = 7, 7 female, Old Age—Early Induction) or late (at 20 m.o., n = 5, 5 female, Old Age—Late Induction) and hippocampi collected at old age (21–22 m.o.). Samples were processed by TRAP and input and positive fraction RNAs collected for RNA seq analysis (Figure 3A). Principal component analysis (PCA) of all expressed genes showed separation by fraction (positive or input) in the first component (67.6% explained variance), but there was no further separation by age of induction or age of collection (Figure 3B). To determine if the timing of Tam induction resulted in similar enrichment of hippocampal microglial translatomes, we compared enrichment (positive fraction/input fraction) of marker genes of various brain cell types[45] following early and late Tam induction. We further compared these data to previously obtained RNA sequencing data from sorted microglial cells as a positive control.[32] TRAP isolated RNA demonstrated equivalent enrichment for microglial marker genes, regardless of induction or collection age, and almost identical enrichment levels as compared to sorted microglial cells (Figure 3C; Tables S2 and S3). Additionally, there was depletion of marker genes for astrocytes, neurons, and oligodendrocytes in the positive fraction as compared to the input (Figures 3C and 3E; Tables S2 and S3). The fold enrichment/depletion for all of these cell type marker genes demonstrated correlations over 0.97 for each age of Tam induction and age of collection (Figure 3D). Overall, these findings demonstrate that microglial RNA enrichment is not affected by the age of Tam induction or collection.

Age of Tam induction does not affect the trajectory of age-related changes in the brain

Once NuTRAP allele induction was determined to be equivalent in both ages of Tam induction and collection, we asked whether timing of Tam induction can affect biological endpoints of importance. We and others have identified significant transcriptional changes in

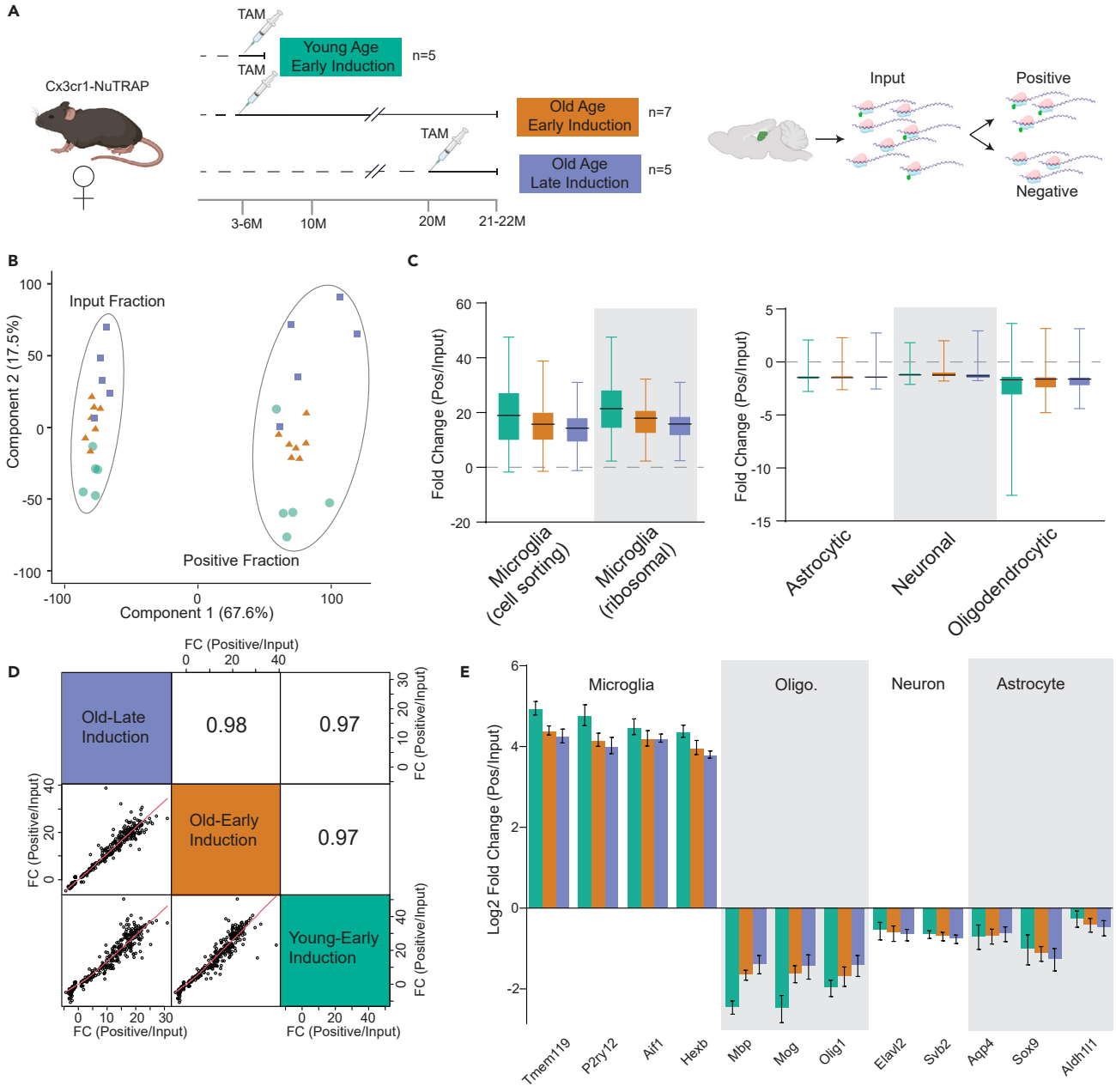

Figure 3. Translatomes from young and old inductions are equivalently enriched for microglial markers

(A) Cx3cr1-NuTRAP mice were induced at 3–6 m.o. and collected at 4 m.o. or 21–22 m.o. or induced at 20 m.o. and collected at 21-22m.o. TRAP isolation was performed on hippocampal dissections and RNASeq profiles generated from Input and Positive fractions.

(B) Translatome profiles separated in the first component between the Input and Positive fractions in the first component and to a degree between young and old mice in the 2nd component.

(C) Assessment of CNS cell type markers derived from cell sorting and ribosomal profiling studies revealed an equivalent enrichment of microglial markers and depletion of markers for other cell types.

(D) Correlation analysis of the union of marker lists demonstrated a high congruency of enrichment (fold change Positive fraction/Input fraction) across ages and ages of TAM induction.

(E) Example marker gene enrichments/depletion for microglia, neuron, astrocyte, and oligodendrocyte markers. Data are presented as mean ± S.E.M.

hippocampal microglia with aging.[40,46,47] We compared gene expression data from the TRAP positive fractions of old mice following early Tam induction (n = 7, 7 females) and old mice following late Tam induction (n = 5, 5 females) to young mice following early Tam induction (n = 5, 5 females) to analyze differential gene expression (One way ANOVA, Benjamini Hochberg Multiple Testing Correction q < 0.1, fold

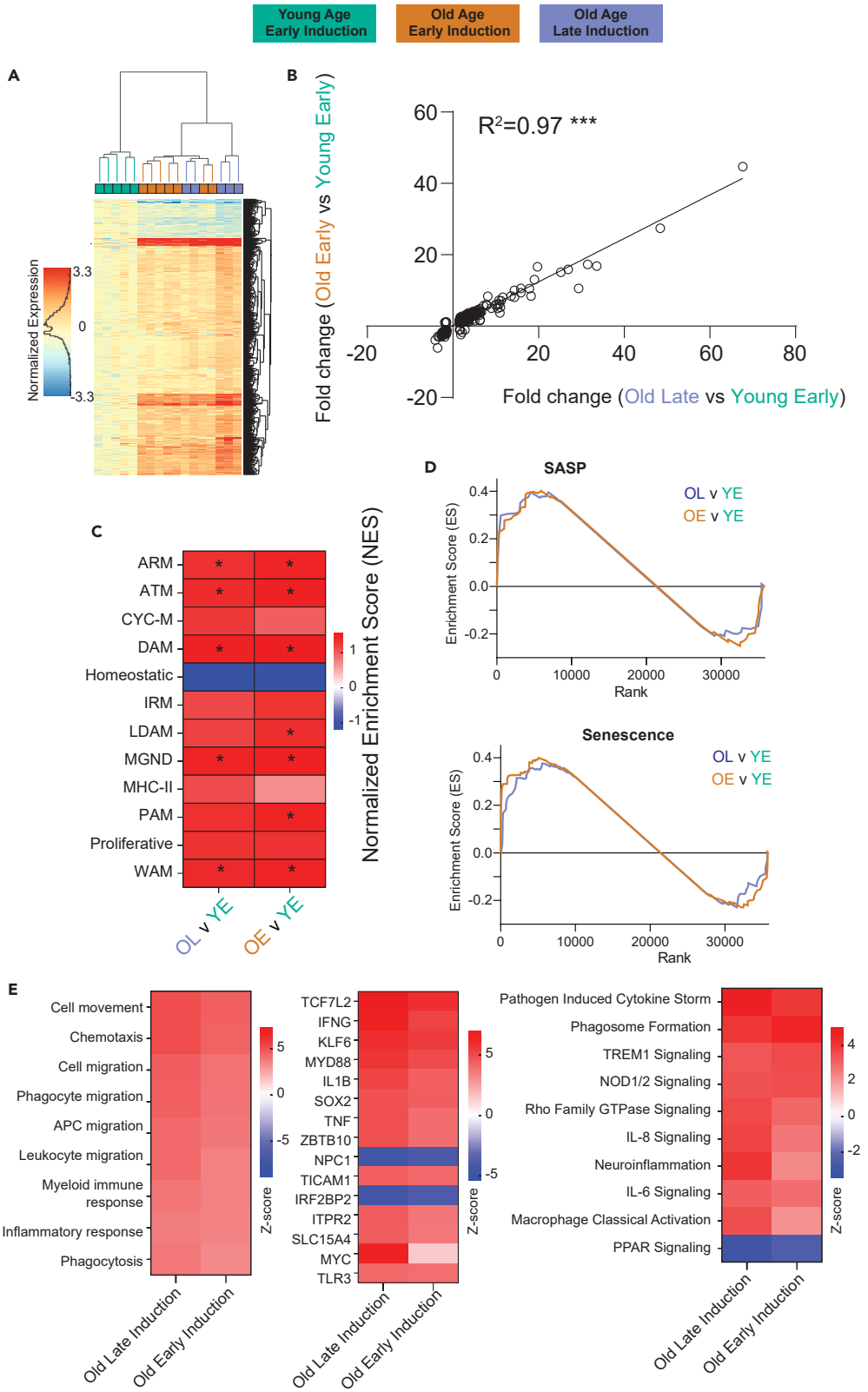
Young Age Early Induction
Old Age Early Induction
Old Age Late Induction
A
Normalized Expression
3.3
0
-3.3
B
R²=0.97 ***
Fold change (Old Early vs Young Early)
Fold change (Old Late vs Young Early)
60
40
20
-20
-20
20
40
60
80
C
ARM
ATM
CYC-M
DAM
Homeostatic
IRM
LDAM
MGND
MHC-II
PAM
Proliferative
WAM
OL v YE
OE v YE
Normalized Enrichment Score (NES)
1
0
-1
D
SASP
OL v YE
OE v YE
Enrichment Score (ES)
0.4
0.2
0.0
-0.2
0
10000
20000
30000
Rank
Senescence
OL v YE
OE v YE
Enrichment Score (ES)
0.4
0.2
0.0
-0.2
0
10000
20000
30000
Rank
E
Cell movement
Chemotaxis
Cell migration
Phagocyte migration
APC migration
Leukocyte migration
Myeloid immune response
Inflammatory response
Phagocytosis
Z-score
5
0
-5
Old Late Induction
Old Early Induction
TCF7L2
IFNG
KLF6
MYD88
IL1B
SOX2
TNF
ZBTB10
NPC1
TICAM1
IRF2BP2
ITPR2
SLC15A4
MYC
TLR3
Z-score
5
0
-5
Old Late Induction
Old Early Induction
Pathogen Induced Cytokine Storm
Phagosome Formation
TREM1 Signaling
NOD1/2 Signaling
Rho Family GTPase Signaling
IL-8 Signaling
Neuroinflammation
IL-6 Signaling
Macrophage Classical Activation
PPAR Signaling
Z-score
4
2
0
-2
Old Late Induction
Old Early Induction

Figure 4. Differentially expressed genes with age are equivalent for different ages of induction

(A) Heatmap of differentially expressed genes comparing both old early induction and old late induction to young early induction mice. The heatmap demonstrates similarity in differential expression in both old groups, allowing for equivalent detection of age-related changes regardless of induction age.

(B) Comparing the age-related fold changes of differentially expressed genes from the different induction ages correlate highly between both ages of induction.

(C) Heatmap of the GSEA enrichment scores comparing enrichment of microglial phenotypic markers (Table S3, gene lists) by tamoxifen induction time (OL v YE) and age (OE v YE) in positive fractions. *p < 0.05 Kolmogorov-Smirnov Test.

(D) GSEA enrichment plots comparing enrichment of senescence associated secretory phenotype (SASP) and senescence markers (Table S3).

(E) Relative *Z* score from IPA for disease pathways, upstream regulators, and canonical pathways for age related changes with various induction ages showing no difference between the old mouse groups.

change >|1.25|) with aging. As visualized by hierarchical clustering, the translatomic differences with age of the two old groups are similar to each other (Figure 4A). This supports that the differential gene profiles with aging of the two old groups are not being significantly affected by age of induction. Differential expression with aging in the old early and late induction, as compared to young, were strongly correlated, with nearly all differentially expressed transcripts demonstrating the same directionality and similar magnitude of change (Figure 4B). Since a few genes have an inverse fold change trend on the plot, we created boxplots of these genes (Figure S2). These few genes demonstrate minor changes between the old early induction and old late induction that may represent random variability. These findings confirm that the Cre induction is not only similar with various ages of induction, but that induction in late age is not inducing confounds and in fact similar populations of microglia are being examined. This supports that different induction ages do not induce confounding variables when using age as an endpoint.

Using the same data, we investigated the relative enrichment of different microglial subtypes with the different ages of induction. Microglia exhibits various phenotypic states[48–51] in response to sterile inflammation with aging. Several subtypes of microglia have been defined, including: (1) disease-associated (DAM),[52] (2) interferon-response (IRM),[53] (3) lipid-droplet (LDAM),[54] (4) white-matter-associated (WAM),[55] (5) activated-response (ARM),[53] (6) neurodegenerative (MGnD),[56] and (7) proliferative-region-associated (PAM)[57] microglia, among others. Recent comparisons have suggested that, perhaps, there are four fundamental patterns underlying these many microglial phenotypes (DAM, IFN, MHC-II, proliferating, etc.).[58] One pattern of note is disease-associated microglia (DAM), first reported[52] and recently reviewed,[59] which are proposed to develop from homeostatic microglia through a progressive change that is initially TREM2-independent (DAM1) and then TREM2-dependent (DAM2). Investigating these various phenotypic states with age is essential to understanding the involvement of microglial inflammation with neurodegeneration, and being able to compare various induction ages of select mouse models with these endpoints is advantageous. As such, we used gene set enrichment analysis (GSEA) to compare microglial phenotypic states of our old mice at different induction ages to our young mice (Figure 4C) using gene sets developed from the literature (Table S3). Comparing old mice to young mice, with both ages of induction, we see an enrichment for reactivated microglial subtypes, such as DAMs, ARMs, MgNDs, and WAMs, while also seeing a depletion of homeostatic microglia. This is consistent with previous findings by our labs and others,[40,54,60] and there is no differential effect due to age of induction.

In addition to microglial phenotypic changes, microglial senescence is emerging as a contributing factor to inflammaging.[61,62] Evidence demonstrates that senescent microglia contribute to cognitive decline and white matter degradation,[63] and this pattern is observed in multiple different microglial subtypes and disease progressions.[40,54,64] We used similar GSEA approaches with senescent cell marker lists (Table S3) to detect enrichment of senescent cells in our aged mice. Both senescent cell type and senescence-associated secretory phenotype (SASP) were enriched in our old mice compared to young, with equivalent enrichment at both induction ages (Figure 4D). This coincides with current research and further supports the effectiveness of using different induction ages of Cre models to investigate various aspects of aging in mice. We further analyzed these data through Ingenuity Pathway Analysis, and there were observed changes in disease pathways, canonical pathways, and upstream regulators associated with aging that were similar regardless of induction age (Figure 4E). While the majority of changes were near identical, there appeared to be some slight differences between the old-late and old-early groups (Figures 4C and 4E). Upon further analysis, we determined these differences to be driven by a few of the old-age mice with slightly higher fold changes in every category. As such, we do not think these differences are attributed to differences caused by induction age and represent natural variability with aging.

Specific microglial responses with age are unaffected by age of Tam induction

For a more focused analysis of the specific changes seen with aging using the different induction ages of the Cre-NuTRAP model, we identified specific cell markers for various conditions or phenotypic states of interest. While enrichment of DAMs was already determined by GSEA, focusing on the most prominent (Figure 5A) DAM markers, there was consistent increase in old samples, regardless of induction age. Examining homeostatic markers, which are known to reduce with age, both ages of induction demonstrated a decrease of homeostatic markers, consistent with expected findings (Figure 5B). Senescent cell markers demonstrated the same pattern, with no effect noted by different induction ages (Figure 5C). We further chose to differentiate between the $p16^{Ink4a}$ and $p19^{Arf}$ isoforms of *Cdkn2a*. $p16^{Ink4a}$ is more associated with senescence and demonstrated a significant increase, consistent between induction ages while $p19^{Arf}$ had smaller increases with age (Figure 5E). In our recent work, we have identified MHC-I components as upregulated with age in microglia from humans, mice, and rats.[46] To assess whether this result is recapitulated with the different induction ages, we analyzed expression of genes for MHC-I and their receptors with early and late Tam induction. We observed increased expression of MHC-I genes *B2m*, *H2-D1*, *H2-K1*, and *H2-M3*, as well as MHC-I receptors, *Lilrb3*, *Lilrb4*, and *Pilra* (Figure 5D). These increases were seen in both induction ages to a similar degree,

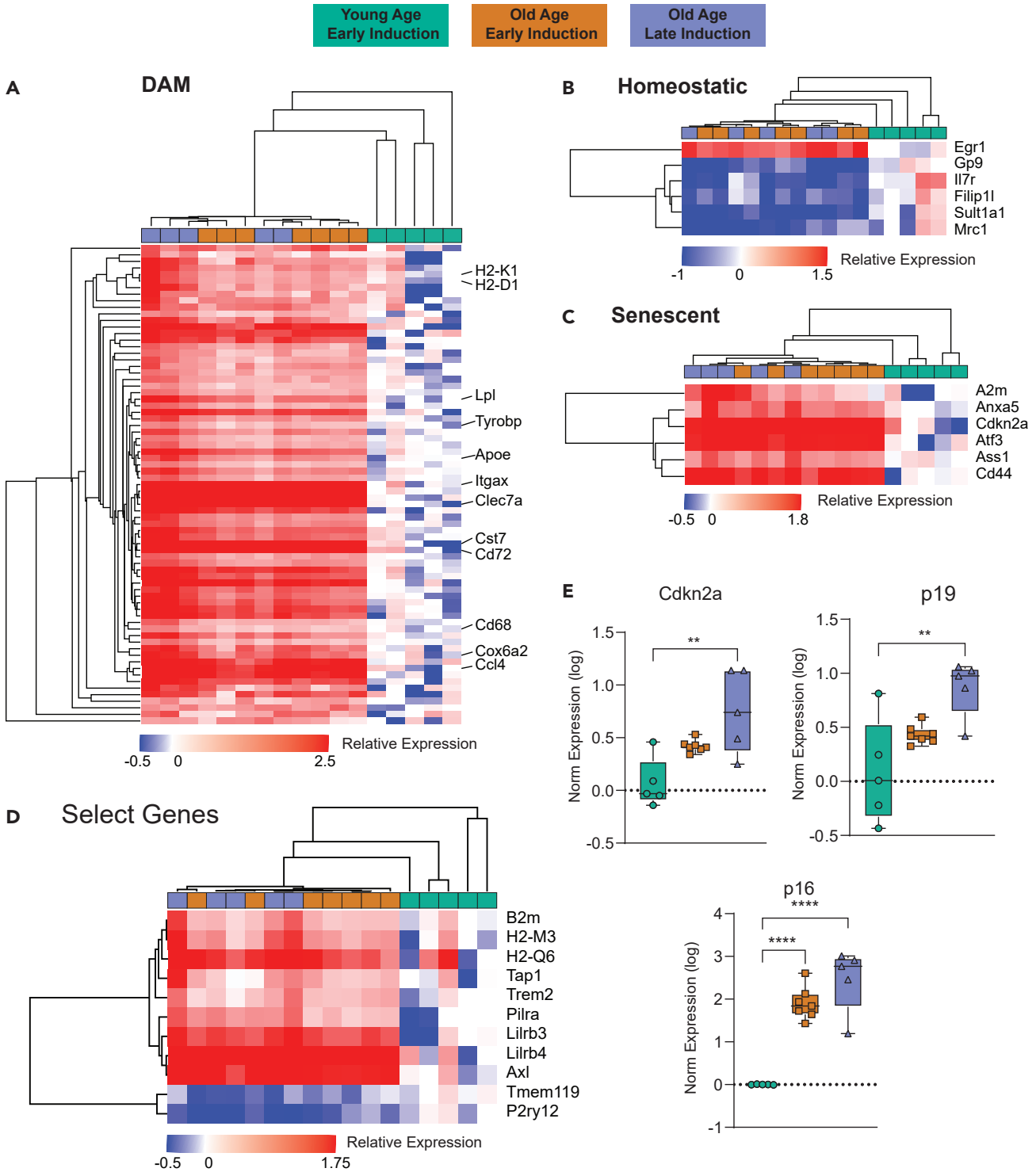

Figure 5. Enrichment of microglial RNA isolated from various ages of induction

(A) Heatmap created from markers for DAMs demonstrating similar enrichment of individual genes for DAMs regardless of age of induction.

(B) Heatmap for homeostatic microglia showing consistent downregulation in both old age groups.

(C) Heatmap for senescence related genes were equivalently upregulated regardless of the age of Tam induction.

(D) Boxplots showing the change with age in both groups of *Cdkn2a* and both of its isoforms, $p19^{Arf}$ and $p16^{Ink4a}$.

(E) Select genes of interest based on other microglial aging studies showing similar patterns of differential expression regardless of age of induction. Data are presented as mean ± S.E.M., One-Way ANOVA SNK post-hoc, **p < 0.01, ****p < 0.0001.

demonstrating the effectiveness of different induction ages that continues to correlate with previous aging data. In a smaller set of male mice (Young n = 4, old-early n = 5, old-late n = 2) we performed a similar analysis and found no/limited differences with age of induction (Figure S3).

DISCUSSION

The focus of this study was to evaluate and characterize the effectiveness of different ages of Tam induction in a Cre/ERT2 mouse model. A microglial NuTRAP mouse model was used to compare induction efficiency and specificity, and to capture age-related changes in the microglial translatome. Tam inducible models have emerged as a critical tool for temporally controlling transgene expression to elucidate gene function, as well as testing the therapeutic potential of different gene targets. In aging research studies, inducing Cre at older ages is potentially highly useful for modulating late-life gene expression without disturbing developmental or adult gene expression. Studies have identified some difference in Tam metabolism with age, sex, and other factors,[19] and a few studies have described limitations and acute negative effects of Tam induction in embryonic and early postnatal models.[23,65] However, to our knowledge there are no studies that have empirically tested for equivalent specificity, efficiency, or consistency of detecting age-related biological changes after inducing cre recombination at older ages. We used a *Cx3cr1-creERT2* driver crossed with a NuTRAP allele as a testing platform that labels microglia and allows for ribosomal isolation to analyze cell type-specific translating RNA.[32] This strategy allows for both identification of labeled cells and assessment of molecular phenotypes. We examined if the Cre induction of our NuTRAP allele maintained the same efficiency and specificity at either early (3–6 m.o.) or late (20 m.o.). Using ribosomal pull-down and translatome sequencing, we then compared expression patterns and the ability to detect age-related changes.

Flow cytometry analysis of eGFP+ cells demonstrated high and equivalent levels of specificity and efficiency at both induction ages. Of note, while efficiency of induction was >90% for Cd11b+ $CD45^{mid}$, presumably microglia, it was lower (~60%) for Cd11b+ $CD45^{high}$ cells which are likely other macrophage cell types. The cell labeling data provide a high degree of confidence that different ages of induction will not cause confounding effects due to differential cre efficiency or specificity.

Molecular analysis of TRAP isolated RNAs allows for an in-depth analysis of cell labeling and for comparison of age-related gene expression changes. Assessment of cell marker lists developed by the field[45] showed equivalent enrichments of microglial markers in young and old mice, and from different induction ages. Additionally, depletion of markers for other cell types was the same between groups. This provides further evidence of similar specificity of microglial labeling across all groups. In analysis of age-related changes, highly consistent alterations in gene expression were observed in old mice as compared to young mice, regardless of the induction age of the old mice. Prototypical signatures of microglial senescence and DAM were evident in old mice. Further, we did see differences between the young and old groups in homeostatic microglial markers (e.g., *P2ry12* and *Tmem119*) which correspond with other studies that demonstrate a reduction in expression of homeostatic markers with age in microglia.[66] The fold changes for age-related changes for the different induction ages were nearly identical, with high correlation. The late induction group had slightly higher fold changes which may be attributable to a batch effect, as this was mainly driven by three of the samples this group collected at the same time. Previously, we have examined the potential for Tam to cause sexually divergent, long-lasting changes in gene expression[67] but found none. We examined males and females in this study. The main findings were in female mice with the analysis of a smaller set of male samples demonstrating the equivalent molecular patterns.

With the concept of antagonistic pleiotropy in the field of Geroscience,[68] and in neurodegeneration research where prodromal versus disease progression studies are needed, the use of Tam inducible Cres in older mice has many applications. For example, C1q is necessary for microglia for development and neuronal pruning, but it can become harmful later in life. Thus C1q-cre studies would benefit from being able to induce the knockout at various ages to better establish the different involvement of C1q at various points in neurodegeneration.[69] Additionally, with the emergence of microglial phenotype analysis, subtypes populations such as DAMs, WAMS, LDAMs, etc. increase with age and may have a protective effect that becomes deleterious.[54] Studies involving these genes and subtype analysis will benefit from changing the *in vivo* genome at different ages to visualize the effects that can only be elucidated in an aged environment.

Limitations of the study

While these findings should be generalizable across Cre/ERT2 systems, it is optimal to test the consistency of specificity, efficiency, and molecular phenotypes that results from cre induction at different ages with each Cre and floxed gene combination. Mouse line specific factors (e.g., cell type, size of flox construct) could alter these results and investigators should also consider using direct assessments of Cre recombination[44] in addition to conventional imaging, flow cytometry, and enrichment tests performed here. However, these results do demonstrate that Tam inducible Cre induction in older mice is a practical approach for aging studies to understand the gene function at different ages.

STAR★METHODS

Detailed methods are provided in the online version of this paper and include the following:

- KEY RESOURCES TABLE
- RESOURCE AVAILABILITY
  - Lead contact
  - Materials availability
  - Data and code availability

SUPPLEMENTAL INFORMATION

Supplemental information can be found online at https://doi.org/10.1016/j.isci.2023.108413.

ACKNOWLEDGMENTS

The authors would like to acknowledge David Bowman for assistance with figure preparation. This work was also supported by grants from the National Institutes of Health (NIH) P30AG050911, R01AG059430, DP5OD033443, T32AG052363, F31AG064861, and R21AG072811. This work was also supported in part by awards I01BX003906, I01BX005396, and IK6BX006033 from the United States (U.S.) Department of Veterans Affairs, Biomedical Laboratory Research and Development Service. The content is solely the responsibility of the authors and does not necessarily represent the official views of the National Institutes of Health. The views expressed in this article are those of the authors and do not necessarily reflect the position or policy of the Department of Veterans Affairs or the United States government.

AUTHOR CONTRIBUTIONS

Conceptualization: W.M.F., M.J.B., A.L.S., and M.B.S.; investigation, C.M.K., K.P., S.K., J.E.J.C., A.D.H., A.J.C.-E., S.R.O., and W.M.F.; statistics and bioinformatics: C.M.K., K.P., S.K., S.R.O., and W.M.F.; writing – original draft, C.M.K., S.K., J.E.J.C., and W.M.F.; writing – review & editing, C.M.K., K.P., S.K., J.E.J.C., A.D.H., M.B.S., A.L.S., M.J.B., A.J.C.-E., S.R.O., and W.M.F.; function acquisition, M.J.B., S.R.O., and W.M.F.

DECLARATION OF INTERESTS

The authors declare they have no financial or non-financial interests directly or indirectly related to this work.

Received: September 19, 2023
Revised: October 15, 2023
Accepted: November 2, 2023
Published: November 9, 2023

REFERENCES

1. Abremski, K., Hoess, R., and Sternberg, N. (1983). Studies on the properties of P1 site-specific recombination: evidence for topologically unlinked products following recombination. Cell *32*, 1301–1311.
2. Sauer, B. (1987). Functional expression of the cre-lox site-specific recombination system in the yeast Saccharomyces cerevisiae. Mol. Cell Biol. *7*, 2087–2096.
3. Feil, R., Wagner, J., Metzger, D., and Chambon, P. (1997). Regulation of Cre recombinase activity by mutated estrogen receptor ligand-binding domains. Biochem. Biophys. Res. Commun. *237*, 752–757.
4. Indra, A.K., Warot, X., Brocard, J., Bornert, J.M., Xiao, J.H., Chambon, P., and Metzger, D. (1999). Temporally-controlled site-specific mutagenesis in the basal layer of the epidermis: comparison of the recombinase activity of the tamoxifen-inducible Cre-ER(T) and Cre-ER(T2) recombinases. Nucleic Acids Res. *27*, 4324–4327.
5. Feil, R., Brocard, J., Mascrez, B., LeMeur, M., Metzger, D., and Chambon, P. (1996). Ligand-activated site-specific recombination in mice. Proc. Natl. Acad. Sci. USA *93*, 10887–10890.
6. Schwenk, F., Kuhn, R., Angrand, P.O., Rajewsky, K., and Stewart, A.F. (1998). Temporally and spatially regulated somatic mutagenesis in mice. Nucleic Acids Res. *26*, 1427–1432.
7. Jahn, H.M., Kasakow, C.V., Helfer, A., Michely, J., Verkhratsky, A., Maurer, H.H., Scheller, A., and Kirchhoff, F. (2018). Refined protocols of tamoxifen injection for inducible DNA recombination in mouse astroglia. Sci. Rep. *8*, 5913.
8. Srinivas, S., Watanabe, T., Lin, C.S., William, C.M., Tanabe, Y., Jessell, T.M., and Costantini, F. (2001). Cre reporter strains produced by targeted insertion of EYFP and ECFP into the ROSA26 locus. BMC Dev. Biol. *1*, 4.
9. Kim, H., Kim, M., Im, S.K., and Fang, S. (2018). Mouse Cre-LoxP system: general principles to determine tissue-specific roles of target genes. Lab. Anim. Res. *34*, 147–159.
10. Sharma, S., and Zhu, J. (2014). Immunologic applications of conditional gene modification technology in the mouse. Curr. Protoc. Immunol. *105*, 10.34.1–10.34.13.
11. Williams, G.C. (1957). Pleiotropy, Natural-Selection, and the Evolution of Senescence. Evolution *11*, 398–411.
12. Tuminello, E.R., and Han, S.D. (2011). The apolipoprotein e antagonistic pleiotropy hypothesis: review and recommendations. Int. J. Alzheimer's Dis. *2011*, 726197.
13. Hashimoto, M., Ho, G., Sugama, S., Takenouchi, T., Waragai, M., Sugino, H., Inoue, S., and Masliah, E. (2021). Possible Role of Activin in the Adiponectin Paradox-Induced Progress of Alzheimer's Disease. J. Alzheimers Dis. *81*, 451–458.
14. Provenzano, F., and Deleidi, M. (2021). Reassessing neurodegenerative disease: immune protection pathways and antagonistic pleiotropy. Trends Neurosci. *44*, 771–780.
15. Wilhelm, T., Byrne, J., Medina, R., Kolundžić, E., Geisinger, J., Hajduskova, M., Tursun, B., and Richly, H. (2017). Neuronal inhibition of the autophagy nucleation complex extends

life span in post-reproductive C. elegans. Genes Dev. *31*, 1561–1572.
16. Schmeisser, K., and Parker, J.A. (2019). Pleiotropic Effects of mTOR and Autophagy During Development and Aging. Front. Cell Dev. Biol. *7*, 192.
17. Chang, L., Andres, M., Sadino, J., Jiang, C.S., Nakama, H., Miller, E., and Ernst, T. (2011). Impact of apolipoprotein E epsilon4 and HIV on cognition and brain atrophy: antagonistic pleiotropy and premature brain aging. Neuroimage *58*, 1017–1027.
18. Jordan, V.C. (2007). New insights into the metabolism of tamoxifen and its role in the treatment and prevention of breast cancer. Steroids *72*, 829–842.
19. Valny, M., Honsa, P., Kirdajova, D., Kamenik, Z., and Anderova, M. (2016). Tamoxifen in the Mouse Brain: Implications for Fate-Mapping Studies Using the Tamoxifen-Inducible Cre-loxP System. Front. Cell. Neurosci. *10*, 243.
20. Cronin-Fenton, D.P., and Damkier, P. (2018). Tamoxifen and CYP2D6: A Controversy in Pharmacogenetics. Adv. Pharmacol. *83*, 65–91.
21. Hu, X.X., Zhou, Q., Lan, T., Huang, X.X., Liang, B.Q., Dai, D.P., Cai, J.P., and Hu, G.X. (2016). Functional characterization of 22 novel CYP2D6 variants for the metabolism of Tamoxifen. J. Pharm. Pharmacol. *68*, 819–825.
22. Yona, S., Kim, K.W., Wolf, Y., Mildner, A., Varol, D., Breker, M., Strauss-Ayali, D., Viukov, S., Guilliams, M., Misharin, A., et al. (2013). Fate mapping reveals origins and dynamics of monocytes and tissue macrophages under homeostasis. Immunity *38*, 79–91.
23. Masuda, T., Amann, L., Sankowski, R., Staszewski, O., Lenz, M., D Errico, P., Snaidero, N., Costa Jordão, M.J., Böttcher, C., Kierdorf, K., et al. (2020). Novel Hexb-based tools for studying microglia in the CNS. Nat. Immunol. *21*, 802–815.
24. McKinsey, G.L., Lizama, C.O., Keown-Lang, A.E., Niu, A., Santander, N., Larpthaveesarp, A., Chee, E., Gonzalez, F.F., and Arnold, T.D. (2020). A new genetic strategy for targeting microglia in development and disease. Elife *9*, e54590.
25. Kaiser, T., and Feng, G. (2019). Tmem119-EGFP and Tmem119-CreERT2 Transgenic Mice for Labeling and Manipulating Microglia. eNeuro *6*, ENEURO.0448,18.2019.
26. Chappell-Maor, L., Kolesnikov, M., Kim, J.S., Shemer, A., Haimon, Z., Grozovski, J., Boura-Halfon, S., Masuda, T., Prinz, M., and Jung, S. (2020). Comparative analysis of CreER transgenic mice for the study of brain macrophages: A case study. Eur. J. Immunol. *50*, 353–362.
27. Parkhurst, C.N., Yang, G., Ninan, I., Savas, J.N., Yates, J.R., 3rd, Lafaille, J.J., Hempstead, B.L., Littman, D.R., and Gan, W.B. (2013). Microglia promote learning-dependent synapse formation through brain-derived neurotrophic factor. Cell *155*, 1596–1609.
28. Goldmann, T., Wieghofer, P., Müller, P.F., Wolf, Y., Varol, D., Yona, S., Brendecke, S.M., Kierdorf, K., Staszewski, O., Datta, M., et al. (2013). A new type of microglia gene targeting shows TAK1 to be pivotal in CNS autoimmune inflammation. Nat. Neurosci. *16*, 1618–1626.
29. Ajami, B., Bennett, J.L., Krieger, C., Tetzlaff, W., and Rossi, F.M.V. (2007). Local self-renewal can sustain CNS microglia maintenance and function throughout adult life. Nat. Neurosci. *10*, 1538–1543.
30. Mildner, A., Schmidt, H., Nitsche, M., Merkler, D., Hanisch, U.K., Mack, M., Heikenwalder, M., Brück, W., Priller, J., and Prinz, M. (2007). Microglia in the adult brain arise from Ly-6ChiCCR2+ monocytes only under defined host conditions. Nat. Neurosci. *10*, 1544–1553.
31. Roh, H.C., Tsai, L.T.Y., Lyubetskaya, A., Tenen, D., Kumari, M., and Rosen, E.D. (2017). Simultaneous Transcriptional and Epigenomic Profiling from Specific Cell Types within Heterogeneous Tissues In Vivo. Cell Rep. *18*, 1048–1061.
32. Chucair-Elliott, A.J., Ocañas, S.R., Stanford, D.R., Ansere, V.A., Buettner, K.B., Porter, H., Eliason, N.L., Reid, J.J., Sharpe, A.L., Stout, M.B., et al. (2020). Inducible cell-specific mouse models for paired epigenetic and transcriptomic studies of microglia and astroglia. Commun. Biol. *3*, 693.
33. Tooley, K.B., Chucair-Elliott, A.J., Ocanas, S.R., Machalinski, A.H., Pham, K.D., Hoolehan, W., Kulpa, A.M., Stanford, D.R., and Freeman, W.M. (2023). Differential usage of DNA modifications in neurons, astrocytes and microglia. Epigenetics Chromatin *16*, 45.
34. Sanz, E., Yang, L., Su, T., Morris, D.R., McKnight, G.S., and Amieux, P.S. (2009). Cell-type-specific isolation of ribosome-associated mRNA from complex tissues. Proc. Natl. Acad. Sci. USA *106*, 13939–13944.
35. Deal, R.B., and Henikoff, S. (2011). The INTACT method for cell type-specific gene expression and chromatin profiling in Arabidopsis thaliana. Nat. Protoc. *6*, 56–68.
36. Heiman, M., Schaefer, A., Gong, S., Peterson, J.D., Day, M., Ramsey, K.E., Suárez-Fariñas, M., Schwarz, C., Stephan, D.A., Surmeier, D.J., et al. (2008). A translational profiling approach for the molecular characterization of CNS cell types. Cell *135*, 738–748.
37. Ocanas, S.R., Pham, K.D., Blankenship, H.E., Machalinski, A.H., Chucair-Elliott, A.J., and Freeman, W.M. (2022). Minimizing the Ex Vivo Confounds of Cell-Isolation Techniques on Transcriptomic and Translatomic Profiles of Purified Microglia. eNeuro *9*, ENEURO.0348-21.2022.
38. Chucair-Elliott, A.J., Ocañas, S.R., Pham, K., Van Der Veldt, M., Cheyney, A., Stanford, D., Gurley, J., Elliott, M.H., and Freeman, W.M. (2022). Translatomic response of retinal Muller glia to acute and chronic stress. Neurobiol. Dis. *175*, 105931.
39. Ocanas, S.R., Isola, J.V.V., Saccon, T.D., Pham, K.D., Chucair-Elliott, A.J., Schneider, A., Freeman, W.M., and Stout, M.B. (2023). Cell-Specific Paired Interrogation of the Mouse Ovarian Epigenome and Transcriptome. J. Vis. Exp. *24*.
40. Ocañas, S.R., Pham, K.D., Cox, J.E.J., Keck, A.W., Ko, S., Ampadu, F.A., Porter, H.L., Ansere, V.A., Kulpa, A., Kellogg, C.M., et al. (2023). Microglial senescence contributes to female-biased neuroinflammation in the aging mouse hippocampus: implications for Alzheimer's disease. J. Neuroinflammation *20*, 188.
41. Crotti, A., and Ransohoff, R.M. (2016). Microglial Physiology and Pathophysiology: Insights from Genome-wide Transcriptional Profiling. Immunity *44*, 505–515.
42. Rangaraju, S., Raza, S.A., Li, N.X., Betarbet, R., Dammer, E.B., Duong, D., Lah, J.J., Seyfried, N.T., and Levey, A.I. (2018). Differential Phagocytic Properties of CD45(low) Microglia and CD45(high) Brain Mononuclear Phagocytes-Activation and Age-Related Effects. Front. Immunol. *9*, 405.
43. Honarpisheh, P., Lee, J., Banerjee, A., Blasco-Conesa, M.P., Honarpisheh, P., d'Aigle, J., Mamun, A.A., Ritzel, R.M., Chauhan, A., Ganesh, B.P., and McCullough, L.D. (2020). Potential caveats of putative microglia-specific markers for assessment of age-related cerebrovascular neuroinflammation. J. Neuroinflammation *17*, 366.
44. Faust, T.E., Feinberg, P.A., O'Connor, C., Kawaguchi, R., Chan, A., Strasburger, H., Frosch, M., Boyle, M.A., Masuda, T., Amann, L., et al. (2023). A comparative analysis of microglial inducible Cre lines. Cell Rep. *42*, 113031.
45. McKenzie, A.T., Wang, M., Hauberg, M.E., Fullard, J.F., Kozlenkov, A., Keenan, A., Hurd, Y.L., Dracheva, S., Casaccia, P., Roussos, P., and Zhang, B. (2018). Brain Cell Type Specific Gene Expression and Co-expression Network Architectures. Sci. Rep. *8*, 8868.
46. Kellogg, C.M., Pham, K., Machalinski, A.H., Porter, H.L., Blankenship, H.E., Tooley, K.B., Stout, M.B., Rice, H.C., Sharpe, A.L., Beckstead, M.J., et al. (2023). Microglial MHC-I induction with aging and Alzheimer's is conserved in mouse models and humans. Geroscience *45*, 3019–3043.
47. Li, H., Ye, T., Liu, X., Guo, R., Yang, X., Li, Y., Qi, D., Wei, Y., Zhu, Y., Wen, L., and Cheng, X. (2023). The role of signaling crosstalk of microglia in hippocampus on progression of ageing and Alzheimer's disease. J. Pharm. Anal. *13*, 788–805.
48. Rock, R.B., Gekker, G., Hu, S., Sheng, W.S., Cheeran, M., Lokensgard, J.R., and Peterson, P.K. (2004). Role of microglia in central nervous system infections. Clin. Microbiol. Rev. *17*, 942–964.
49. Avignone, E., Lepleux, M., Angibaud, J., and Nägerl, U.V. (2015). Altered morphological dynamics of activated microglia after induction of status epilepticus. J. Neuroinflammation *12*, 202.
50. Dubbelaar, M.L., Kracht, L., Eggen, B.J.L., and Boddeke, E.W.G.M. (2018). The Kaleidoscope of Microglial Phenotypes. Front. Immunol. *9*, 1753.
51. Provenzano, F., Pérez, M.J., and Deleidi, M. (2021). Redefining Microglial Identity in Health and Disease at Single-Cell Resolution. Trends Mol. Med. *27*, 47–59.
52. Keren-Shaul, H., Spinrad, A., Weiner, A., Matcovitch-Natan, O., Dvir-Szternfeld, R., Ulland, T.K., David, E., Baruch, K., Lara-Astaiso, D., Toth, B., et al. (2017). A Unique Microglia Type Associated with Restricting Development of Alzheimer's Disease. Cell *169*, 1276–1290.e17.
53. Sala Frigerio, C., Wolfs, L., Fattorelli, N., Thrupp, N., Voytyuk, I., Schmidt, I., Mancuso, R., Chen, W.T., Woodbury, M.E., Srivastava, G., et al. (2019). The Major Risk Factors for Alzheimer's Disease: Age, Sex, and Genes Modulate the Microglia Response to Aβ Plaques. Cell Rep. *27*, 1293–1306.e6.
54. Marschallinger, J., Iram, T., Zardeneta, M., Lee, S.E., Lehallier, B., Haney, M.S., Pluvinage, J.V., Mathur, V., Hahn, O., Morgens, D.W., et al. (2020). Lipid-droplet-accumulating microglia represent a dysfunctional and proinflammatory state in the aging brain. Nat. Neurosci. *23*, 194–208.
55. Safaiyan, S., Besson-Girard, S., Kaya, T., Cantuti-Castelvetri, L., Liu, L., Ji, H., Schifferer, M., Gouna, G., Usifo, F., Kannaiyan, N., et al. (2021). White matter aging drives microglial diversity. Neuron *109*, 1100–1117.e10.

56. Krasemann, S., Madore, C., Cialic, R., Baufeld, C., Calcagno, N., El Fatimy, R., Beckers, L., O'Loughlin, E., Xu, Y., Fanek, Z., et al. (2017). The TREM2-APOE Pathway Drives the Transcriptional Phenotype of Dysfunctional Microglia in Neurodegenerative Diseases. Immunity *47*, 566–581.e9.
57. Li, Q., Cheng, Z., Zhou, L., Darmanis, S., Neff, N.F., Okamoto, J., Gulati, G., Bennett, M.L., Sun, L.O., Clarke, L.E., et al. (2019). Developmental Heterogeneity of Microglia and Brain Myeloid Cells Revealed by Deep Single-Cell RNA Sequencing. Neuron *101*, 207–223.e10.
58. Chen, Y., and Colonna, M. (2021). Microglia in Alzheimer's disease at single-cell level. Are there common patterns in humans and mice? J. Exp. Med. *218*, e20202717.
59. Deczkowska, A., Keren-Shaul, H., Weiner, A., Colonna, M., Schwartz, M., and Amit, I. (2018). Disease-Associated Microglia: A Universal Immune Sensor of Neurodegeneration. Cell *173*, 1073–1081.
60. Hammond, T.R., Dufort, C., Dissing-Olesen, L., Giera, S., Young, A., Wysoker, A., Walker, A.J., Gergits, F., Segel, M., Nemesh, J., et al. (2019). Single-Cell RNA Sequencing of Microglia throughout the Mouse Lifespan and in the Injured Brain Reveals Complex Cell-State Changes. Immunity *50*, 253–271.e6.
61. Franceschi, C., and Campisi, J. (2014). Chronic inflammation (inflammaging) and its potential contribution to age-associated diseases. J. Gerontol. A Biol. Sci. Med. Sci. *69*, S4–S9.
62. Monti, D., Ostan, R., Borelli, V., Castellani, G., and Franceschi, C. (2017). Inflammaging and human longevity in the omics era. Mech. Ageing Dev. *165*, 129–138.
63. Ahn, K., Lee, S.J., and Mook-Jung, I. (2022). White matter-associated microglia: New players in brain aging and neurodegenerative diseases. Ageing Res. Rev. *75*, 101574.
64. Liu, R.M. (2022). Aging, Cellular Senescence, and Alzheimer's Disease. Int. J. Mol. Sci. *23*, 1989.
65. Ilchuk, L.A., Stavskaya, N.I., Varlamova, E.A., Khamidullina, A.I., Tatarskiy, V.V., Mogila, V.A., Kolbutova, K.B., Bogdan, S.A., Sheremetov, A.M., Baulin, A.N., et al. (2022). Limitations of Tamoxifen Application for In Vivo Genome Editing Using Cre/ER(T2) System. Int. J. Mol. Sci. *23*, 14077.
66. Hajdarovic, K.H., Yu, D., Hassell, L.A., Evans, S., Packer, S., Neretti, N., and Webb, A.E. (2022). Single-cell analysis of the aging female mouse hypothalamus. Nat. Aging *2*, 662–678.
67. Chucair-Elliott, A.J., Ocanas, S.R., Stanford, D.R., Hadad, N., Wronowski, B., Otalora, L., Stout, M.B., and Freeman, W.M. (2019). Tamoxifen induction of Cre recombinase does not cause long-lasting or sexually divergent responses in the CNS epigenome or transcriptome: implications for the design of aging studies. Geroscience *41*, 691–708.
68. Leroi, A.M., Bartke, A., De Benedictis, G., Franceschi, C., Gartner, A., Gonos, E.S., Fedei, M.E., Kivisild, T., Lee, S., Kartaf-Ozer, N., et al. (2005). What evidence is there for the existence of individual genes with antagonistic pleiotropic effects? Mech. Ageing Dev. *126*, 421–429.
69. Fonseca, M.I., Chu, S.H., Hernandez, M.X., Fang, M.J., Modarresi, L., Selvan, P., MacGregor, G.R., and Tenner, A.J. (2017). Cell-specific deletion of C1qa identifies microglia as the dominant source of C1q in mouse brain. J. Neuroinflammation *14*, 48.
70. Sahasrabuddhe, V., and Ghosh, H.S. (2022). Cx3Cr1-Cre induction leads to microglial activation and IFN-1 signaling caused by DNA damage in early postnatal brain. Cell Rep. *38*, 110252.
71. Clark, N.R., and Ma'ayan, A. (2011). Introduction to statistical methods for analyzing large data sets: gene-set enrichment analysis. Sci. Signal. *4*, tr4.
72. Krämer, A., Green, J., Pollard, J., Jr., and Tugendreich, S. (2014). Causal analysis approaches in Ingenuity Pathway Analysis. Bioinformatics *30*, 523–530.

STAR★METHODS

KEY RESOURCES TABLE

REAGENT or RESOURCE	SOURCE	IDENTIFIER
Antibodies		
Anti-GFP antibody	Abcam	Cat# ab290; RRID:AB_303395
CD11b Antibody, anti-human/mouse	Miltenyi Biotec	Cat# 130-113-793; RRID:AB_2726317
CD45 Antibody, anti-mouse, REAfinity	Miltenyi Biotec	Cat# 130-110-802; RRID:AB_2658222
Anti-mCherry antibody	Abcam	Cat # ab167453; RRID:AB_2571870
Anti-Mouse CD11b	Leinco	Cat # C227; RRID:AB_2829357
Chemicals, peptides, and recombinant proteins		
Cycloheximide solution	MilliporeSigma	C4859
RNaseOUT Recombinant Ribonuclease Inhibitor	Thermo Fisher Scientific	10777019
Spermidine	MilliporeSigma	S2626
cOmplete, Mini, EDTA-free Protease Inhibitor Cocktail	MilliporeSigma	11836170001
Dynabeads Protein G for Immunoprecipitation	Thermo Fisher Scientific	10003D
β-Mercaptoethanol, Molecular Biology Grade	MilliporeSigma	444203
DPBS, calcium, magnesium, glucose, pyruvate	Thermo Fisher Scientific	14287–072
Actinomycin D	MilliporeSigma	A1410
Triptolide	MilliporeSigma	T3652
Anisomycin from *Streptomyces griseolus*	MilliporeSigma	A9789
Debris Removal Solution	Miltenyi Biotec	130-109-398
MACS BSA Stock Solution	Miltenyi Biotec	130-091-376
SPRIselect	Beckman Coulter	B23318
Critical commercial assays		
Qiagen, Inc. RNeasy Mini Kit, 50 RNeasy Mini Spin Columns	QIAGEN	74104
Adult Brain Dissociation Kit, mouse and rat	Miltenyi Biotec	130-107-677
NEBNext Ultra II Directional RNA Library Prep Kit for Illumina	New England Biolabs	NEBE7760
Qubit 1X dsDNA High Sensitivity (HS) and Broad Range (BR) Assay Kits	Thermo Fisher Scientific	Q33230
Deposited data		
RNA Sequencing Source Data generated for this study	GEO	GSE241574
RNA Sequencing Source Data from previous study	GEO	GSE233400
Experimental models: Organisms/strains		
Mouse: Cx3cr1^{Jung}: B6.129P2(Cg)-*Cx3cr1*$^{tm2.1(cre/ERT2)Litt}$/WganJ	Jax	020940
Mouse: NuTRAP: B6; 129S6-*Gt(ROSA)26Sor*$^{tm2(CAG-NuTRAP)Evdr}$/J	Jax	029899
Mouse: Cx3cr1-cre; NuTRAP: Cx3cr1$^{Jung\text{-}cre/ERT2+/wt}$; NuTRAP$^{flox/wt}$	Breeding at OMRF	N/A; Bred between 021160 and 029899
Oligonucleotides		
generic Cre Forward	Jax	oIMR8346
generic Cre Reverse	Jax	19974
+ ctl Forward	Jax	oIMR7338
+ctl Rev	Jax	oIMR7339
Cx3cr1 Jung Mutant Forward	Jax	21059
Cx3cr1 Jung Common	Jax	21058
Cx3cr1 Jung WT Forward	Jax	20669
Index Primers for RNA Sequencing	New England Biolabs	E6609L

(*Continued on next page*)

Continued

REAGENT or RESOURCE	SOURCE	IDENTIFIER
Deposited data		
	Gene Expression Omnibus	GSE241574
	Gene Expression Omnibus	GSE233400

RESOURCE AVAILABILITY

Lead contact

Further information and requests for resources and reagents should be directed to and will be fulfilled by the lead contact, Willard M. Freeman (bill-freeman@omrf.org).

Materials availability

Mouse lines used in this in this study are available from Jackson Laboratory (*Cx3cr1*$^{Jung\text{-}Cre/ERT2+/+}$ (stock #020940) and *NuTRAP*$^{flox/flox}$ females (stock # 029899).

Data and code availability

The entirety of the RNA sequencing data have been deposited in FASTQ format at the NCBI Gene Expression Omnibus and are publicly available as of the date of publication. Accession numbers are listed in the key resources table. This paper does not report original code. Any additional information required to reanalyze the data reported in this paper is available from the lead contact upon request.

EXPERIMENTAL MODEL AND STUDY PARTICIPANT DETAILS

Mice

All animal procedures were approved by the Oklahoma Medical Research Foundation (OMRF) Institutional Animal Care and Use Committee. Breeder mice were purchased from Jackson Laboratory (Bar Harbor, ME), bred, and housed at the OMRF, under pathogen free conditions in a HEPA barrier environment. *Cx3cr1*$^{Jung\text{-}Cre/ERT2+/+}$ (stock #020940)[22] males were mated with *NuTRAP*$^{flox/flox}$ females (stock # 029899)[31] to generate the desired progeny, *Cx3cr1*$^{Jung\text{-}cre/ERT2+/wt}$; *NuTRAP*$^{flox/wt}$.[32] Both of these strains are from the C57BL/6J background. Intraperitoneal (IP) injections of tamoxifen (Tam) solubilized by sonication in 100% sunflower seed oil (100 mg/kg body weight, 20 mg/mL stock solution, #T5648; Millipore Sigma, St. Louis, MO) were administered daily for five consecutive days[32] at the specified ages. Tam induction at 3 m.o. and older does not lead to long-lasting changes in brain gene expression[67] and avoids potential confounds of early post-natal Tam administration in microglial studies.[70] Based on an average weight of 20 g per mouse, each Tam injection consisted of 100 μL of 20 mg/mL stock solution. Adjustments were made for mice that significantly deviated from the average weight. Mice were euthanized by cervical dislocation, followed by rapid decapitation, in line with the AVMA Guidelines for the Euthanasia of Animals. Tam induction was performed at early (3–6 m.o.) or late age (20 m.o.).

Mouse genotyping

DNA was extracted from mouse ear punch samples by incubating samples in 50 nM NaOH at 95°C for 1 h, after which the reaction was neutralized by adding 30 μL 1 M Tris HCl (pH: 7.4). Genotyping was performed by touchdown PCR (94°C hotstart for 2 min, 10 cycles of touchdown (94°C 20 s, 65°C 15 s (−0.5C per cycle decrease per cycle)), 68°C,10 s) followed by 28 cycles of amplification (94°C 15 s, 60°C 15 s, 72°C 10 s) with the listed primer sets (Table S1).

METHOD DETAILS

TRAP isolation

*M*inced hippocampal tissue was Dounce homogenized (#D8938; MilliporeSigma) in 1.5 mL chilled homogenization buffer (50 mM Tris, pH 7.4; 12 mM $MgCl_2$; 100 mM KCl; 1% NP-40; 1 mg/mL sodium heparin; 1 mM DTT; 100 μg/mL cycloheximide [#C4859-1ML, MilliporeSigma]; 200 units/mL RNaseOUT Recombinant Ribonuclease Inhibitor [#10777019; Thermo Fisher Scientific]; 0.5 mM Spermidine [#S2626, MilliporeSigma]; 1× complete EDTA-free Protease Inhibitor Cocktail [#11836170001; MilliporeSigma]).[32] Homogenates were transferred to 2 mL round-bottom tubes and centrifuged at 12,000 × g for 10 min at 4°C. 100 μL of supernatant was saved as "Input." The remaining supernatant was transferred to a 2-mL round-bottom tube and incubated with 5 μg/μL of anti-EGFP antibody (ab290; Abcam) at 4°C with end-over-end rotation for 1 h. Dynabeads Protein G for IP (#10003D; Thermo Fisher Scientific) were pre-washed three times in 1-mL ice-cold low-salt wash buffer (50 mM Tris, pH 7.5; 12 mM $MgCl_2$; 100 mM KCl; 1% NP-40; 100 μg/mL cycloheximide; 1 mM DTT). The homogenate/antibody mixture was transferred to the 2-mL round-bottom tube containing the washed Protein-G Dynabeads and incubated at 4°C with end-over-end rotation overnight. Magnetic beads were collected (DynaMag-2 magnet) and the unbound-ribosomes and associated RNA discarded. Beads and eGFP-bound polysomes were then washed 3X with 0.5 mL of high-salt wash buffer (50 mM Tris, pH 7.5; 12 mM $MgCl_2$; 300 mM KCl; 1% NP-40;

100 μg/mL cycloheximide; 2 mM DTT). Following the last wash, 350 μL of buffer RLT (QIAGEN) supplemented with 3.5 μL 2-β mercaptoethanol (#444203, MilliporeSigma) was added directly to the beads and incubated with mixing on a ThermoMixer (Eppendorf) for 10 min at room temperature. The beads were magnetically separated and the supernatant containing the target bead-bound polysomes and associated RNA was transferred to a new tube and constitutes the positive fraction for subsequent analysis. A total of 350 μL of 100% ethanol was added to the sample and loaded onto an RNeasy MinElute column (QIAGEN). RNA was isolated using RNeasy Mini kit (#74104, QIAGEN), and quantified with a Nanodrop One^{c} spectrophotometer (#ND-ONEC-W, Thermo Fisher Scientific) and quality assessed by HSRNA ScreenTape (#5067–5579, Agilent Technologies) with a 4150 Tapestation analyzer (#G2992AA, Agilent Technologies).

Single cell suspension

Adjacent cortex tissue from the same Cx3cr1-NuTRAP mice used for hippocampal TRAP-Seq analyses were collected for flow cytometric analyses. The tissue was rinsed in ice-cold D-PBS containing calcium, magnesium, glucose, and pyruvate (#14287-072, Thermo Fisher Scientific), minced, and placed into ice-cold gentleMACS C-tubes (#130-093-237, Miltenyi Biotec), containing 1950 μL of Enzyme Mix 1. For each reaction, Enzyme Mix 1 was created by combining 50 μL of Enzyme P with 1900 μL of buffer Z, while Enzyme Mix 2 was created by combining 10 μL of Enzyme A with 20 μL of buffer Y per reaction, with all reagents included in the Adult Brain Dissociation kit (#130-107-677, Miltenyi Biotec). Transcription and translation inhibitors were included during cell preparation to prevent *ex vivo* activational artifacts.[37] Actinomycin D (#A1410, MilliporeSigma) was reconstituted in DMSO at 5 mg/mL before being aliquoted and stored at −20°C protected from light. Triptolide (#T3652, MilliporeSigma) was reconstituted in DMSO to a concentration of 10 mM before being aliquoted and stored at −20°C protected from light. Anisomycin (#A9789, MilliporeSigma) was reconstituted in DMSO to a concentration of 10 mg/mL before being aliquoted and stored at 4°C protected from light. 2 μL each of actinomycin D, triptolide, and anisomycin stocks were added to the initial Enzyme Mix 1 before dissociation for a final concentration of 5 μg/mL, 10 μM, and 10 μg/mL, respectively. Each sample had 30 μL of Enzyme Mix 2 added before being mechanically dissociated for 30 min at 37°C on the gentleMACS Octo Dissociator with Heaters (#130-096-427, Miltenyi Biotec) using the 37C_ABDK_02 program. Following enzymatic and mechanical dissociation, the C-tubes were quickly spun in a chilled (4°C) Allegra-30R centrifuge (#B08708, Beckman Coulter) with an SX4400 swinging bucket rotor to collect the samples in the bottom of the tubes. Next, samples were resuspended, passed through a pre-wet 70 μm MACS SmartStrainer (#130-110-916, Miltenyi Biotec), and collected in a 50-mL conical tube (#21008-178, VWR International). The C-tubes were washed with 10 mL of ice-cold D-PBS, and the washed volume was passed through the 70 μm MACS SmartStrainer. The cells were then pelleted by centrifugation at 300 × g for 10 min at 4°C. Following centrifugation, the supernatant was aspirated and debris was removed using the Debris Removal solution (#130-109-398, Miltenyi Biotec) provided in the Adult Brain Dissociation kit (#130-107-677, Miltenyi Biotec). Briefly, cells were resuspended in 1.55 mL of ice-cold D-PBS and passed to a 5-mL round bottom tube (#22171606, FisherScientific), and 450 μL of cold Debris Removal solution was mixed into the cell suspensions. Next, 2 mL of D-PBS was gently overlaid on the cell suspension, ensuring the layers did not mix. Centrifugation at 3000 × g for 10 min at 4°C separated the suspension into three phases, of which the top two phases were aspirated. The cell pellet was gently resuspended in 5 mL of ice-cold D-PBS before centrifugation at 1000 × g for 10 min at 4°C. After aspirating the supernatant completely, the cells were resuspended in 1 mL 0.5% BSA (#130-091-376, Miltenyi Biotec) in D-PBS and filtered through a 35-μm filter (#352235, Fisher Scientific).

RNA-seq

Directional RNA-Seq libraries (NEBNext Ultra II Directional RNA Library, New England Biolabs, Ipswich, MA NEB#E7760) were constructed.[37] Poly-adenylated RNA was captured using NEBNext Poly(A) mRNA Magnetic Isolation Module (#NEBE7490). Following mRNA capture, mRNA was eluted from the oligo-dT beads and fragmented by incubating with the First Strand Synthesis Reaction buffer and Random Primer Mix (2×) from the NEBNext Ultra II Directional Library Prep Kit for Illumina (#NEBE7760; New England Biolabs) for 15 min at 94°C. First and second strand cDNA synthesis were performed sequentially, as instructed by the manufacturer's guidelines. After purification of double-stranded cDNA with 1.8× SPRISelect Beads (#B23318, Beckman Coulter), purified cDNA was eluted in 50 μL 0.1× TE buffer and subjected to end prep. The NEBNext adaptor was diluted 1:100 in Adaptor Dilution buffer (provided) before ligating the adaptor to the cDNA. After purifying the ligation reaction with 0.9× SPRISelect Beads (#B23318, Beckman Coulter), cDNA was eluted in 15 μL of 0.1× TE (provided). Next, cDNA libraries were amplified with 16 cycles of PCR using the NEBNext Ultra II Q5 Master Mix (provided) and unique index primer mixes from NEBNext Multiplex Oligos for Illumina Library (#E6609L, New England Biolabs). Libraries were purified with 0.9× SPRISelect Beads (#B23318, Beckman Coulter) and then sized with HSD1000 ScreenTapes (#5067–5584; Agilent Technologies). Libraries had an average peak size of 316 bp. Libraries were quantified by Qubit 1× dsDNA HS Assay kit (#Q33230, Thermo Fisher Scientific). The libraries for each sample were pooled at 4 nm concentration and sequenced using an Illumina NovaSeq 6000 system (S4 PE150).

Flow cytometry

For flow cytometric analysis, cell preparations were analyzed on a MACSQuant Analyzer 10 Flow Cytometer.[37] Cells were stained with CD11b-APC (M1/70, #130-113-793, Miltenyi Biotec) and CD45-VioBlue (REA737, #130-110-802, Miltenyi Biotec). Following staining, cells were resuspended in 250 μL of 0.5% BSA/D-PBS. Data were analyzed using MACSQuantify v2.13.0 software.

Immunohistochemistry

For immunohistochemistry (IHC), mouse brains were hemisected and processed for cryosectioning.[32,37] Samples were fixed for a duration of 4h in 4% PFA, cryoprotected by overnight incubation in PBS containing 30% sucrose, and then frozen in Optimal Cutting Temperature medium (Tissue-Tek, #4583). Ten μm-thick sagittal sections were cryotome-cut and sections containing the hippocampus at the level of dentate gyrus were collected (Cryostar NX70, ThermoFisher Scientific). Tissue sections were rinsed with PBS containing 1% Triton X-100, blocked for 1h in PBS containing 10% normal donkey serum, and processed for fluorescence immunostaining. The primary antibodies included rabbit anti-mCherry (#ab167453, 1:500, Abcam, Cambridge, MA) and rat anti-CD11b (#C227, 1:200, Leinco Technologies, St. Louis, MO). Sequential imaging of brain samples was performed on an Olympus FluoView confocal laser-scanning microscope (FV1200; Olympus; Center Valley, PA) at the Dean McGee Eye Institute (DMEI) imaging core facility at the Oklahoma University Health Sciences Center (OUHSC). Microscope and FLUOVIEW FV1000 v1.2.6.0 software (Olympus) settings were identical for all samples at same magnification. The z stack generated was achieved at 1.26 μm step size with a total of 6 optical slices at 40X magnification (1.2× zoom). Raw images used for figure assembly were processed using Adobe Photoshop (v24.7.0).

QUANTIFICATION AND STATISTICAL ANALYSIS

RNA-seq data analysis

Following sequencing, reads were trimmed and aligned before differential expression statistics and correlation analyses in Strand NGS software package (v4.0; Strand Life Sciences). Reads were aligned against the full mm10 genome build (2014.11.26). Alignment and filtering criteria included the following: adapter trimming, fixed 2-bp trim from 5′ and 2-bp from 3′ ends, a maximum number of one novel splice allowed per read, a minimum of 90% identity with the reference sequence, a maximum 5% gap, and trimming of 3′ ends with $Q < 30$. Alignment was performed directionally with Read 1 aligned in reverse and Read 2 in forward orientation. All duplicate reads were then removed. Normalization was performed with the DESeq2 algorithm. Transcripts with an average read count value > 20 in at least 100% of the samples in at least one group were considered expressed at a level sufficient for quantitation per tissue and those transcripts below this level were considered not detected/not expressed and excluded, as these low levels of reads are close to background and are highly variable. For statistical analysis of differential expression with aging a One-Way ANOVA with Benjamini–Hochberg multiple testing correction (BHMTC) was performed with Student–Newman–Keuls pairwise post-hoc testing. For those transcripts meeting this statistical criterion, a fold change >|1.25| cutoff was used to eliminate those genes which were statistically significant but unlikely to be biologically significant and orthogonally confirmable because of their very small magnitude of change. Visualizations of hierarchical clustering and principal component analyses (PCAs) were performed in Strand NGS (version 4.0). Gene set enrichment analysis (GSEA) was performed using GSEA v4.3.2. Heatmaps of the GSEA enrichment scores were made using Morpheus software (https://software.broadinstitute.org/morpheus).

Statistical analysis

Statistical analysis of RNA-Seq data was performed as described above using a One-Way ANOVA using a Benjamini Hochberg Multiple Testing Correction with n = 5 Young Early Induction, n = 7 Old Early Induction, and n = 5 Old Late Induction, where each sample is an independent biological sample/mouse. For analysis of flow cytometry data (n = 6 Early Induction, n = 7 Late Induction) a One-Way ANOVA with Student–Newman–Keuls pairwise post-hoc testing performed, $\alpha < 0.05$. Gene Set Enrichment Analysis statistical assessment was performed with Kolmogorov-Smirnov test.[71] Ingenuity Pathway Analysis was performed with *Z* score analysis.[72]